

Ambivalent effects of added layers on steady kinematic dynamos in cylindrical geometry: application to the VKS experiment

F. Stefani ^{a,*}, M. Xu ^a, G. Gerbeth ^a, F. Ravelet ^b
A. Chiffaudel ^b, F. Daviaud ^b, J. Léorat ^c

^a*Forschungszentrum Rossendorf, P.O. Box 510119, D-01314 Dresden, Germany*

^b*Service de Physique de l'État Condensé, DSM, CEA Saclay, CNRS URA 2464, 91191 Gif-sur-Yvette, France*

^c*LUTH, Observatoire de Paris-Meudon, 92195 Meudon, France*

Abstract

The intention of the "von Kármán sodium" (VKS) experiment is to study the hydromagnetic dynamo effect in a highly turbulent and unconstrained flow. Much effort has been devoted to the optimization of the mean flow and the lateral boundary conditions in order to minimize the critical magnetic Reynolds number R_m^c and hence the necessary motor power. The main focus of this paper lies on the role of "lid layers", i.e. layers of liquid sodium between the impellers and the end walls of the cylinder. First, we study an analytical test flow to show that lid layers can have an ambivalent effect on the efficiency of the dynamo. The critical magnetic Reynolds number shows a flat minimum for a small lid layer thickness, but increases for thicker layers. For the actual VKS geometry it is shown that static lid layers yield a moderate increase of R_m^c by approximately 12 per cent. A more dramatic increase by 100 till 150 per cent can occur when some rotational flow is taken into account in those layers. Possible solutions of this problem are discussed for the real dynamo facility.

Key words: Magnetic field; Dynamo experiments; Integral equations

* Corresponding author. e-mail: F.Stefani@fz-rossendorf.de

1 Introduction

The Earth's magnetic field, as most other cosmic magnetic fields, is generated by the hydromagnetic dynamo effect. [1]. The dynamo effect is an instability of the magnetic field in a flow of conducting liquid, which is controlled by the magnetic Reynolds number $R_m = \mu\sigma LV$, where μ is the magnetic permeability of the fluid (which is, in most cases, equal to the permeability of the vacuum, μ_0), σ the electrical conductivity of the fluid, and L and V are typical length and velocity scales of the flow, respectively. Typical values of the critical R_m are in the order 10 till 100. A comparably simple way to reach such values is the use of materials with high relative permeability. Indeed, this was done by Lowes and Wilkinson in the sixties. Their first successful homogeneous dynamos comprised two Perminvar cylinders spinning around non-parallel axes in a "house-shaped" surrounding conductor [2,3]. Although being genuine homogeneous dynamos, they did not allow to study non-trivial back-reaction effects as they are typical for the *hydromagnetic* dynamos in the cosmos.

The first experimental realisation of such hydromagnetic dynamos was left to 1999 [4], when magnetic field self-excitation was observed in two large-size liquid sodium facilities in Riga [5,6] and Karlsruhe [7,8]. Since that time, both experiments have brought about a wealth of data on the kinematic and the saturated regime. In both cases, the comparison of the experimental results with the numerical predictions shows a satisfactory agreement. In contrast to electro-technical dynamos which are characterized by an abrupt saturation at the critical rotation rate due to their constructional stiffness, hydromagnetic dynamos saturate in a much "softer" way due to the deformability of the flow structure. This has been shown, in particular, at the Riga experiment [9], where the back-reaction of the magnetic field acts very selectively on the azimuthal velocity component. This flow deformation explains the very flat increase of the Joule power above the self-excitation threshold.

While both the kinematic dynamo effect and the non-trivial saturation mechanism (due to flow deformation) have been investigated in the Riga experiment, there are still open questions which are better addressed in the framework of other experimental facilities. One of the most important issues concerns the role of high levels of turbulence on the self-excitation condition, a problem that can hardly be solved by theory and numerics alone.

Besides other experimental efforts at different sites in the world [4], the VKS project in Cadarache, France, is one of the most promising candidates to meet this goal [10,11,12]. The acronym "VKS" stands for "von Kármán sodium" and refers to a flow that is produced between two counter-rotating impellers in a finite cylinder (cf. Fig. 1). The impellers consist of flat disks fitted with

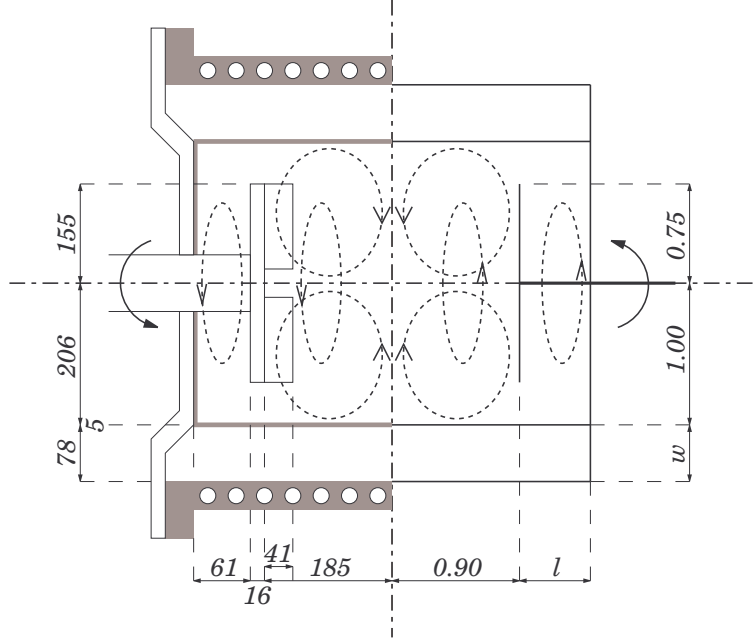


Fig. 1. Principle design, flow structure, and dimensions of the VKS experiment. The two impellers produce two counter-rotating toroidal eddies and, by centrifugal pumping, two poloidal rolls. Left half: Technical details, including the main vessel with the cooling system, the copper envelope, the impeller with attached blades and its shaft. Copper parts are gray, stainless steel parts are white. The indicated dimensions are in mm. Right half: Simplified geometry as it is assumed in the numerical simulations with dimensionless lengths. The dimensionless thicknesses of the side layer and the lid layer are denoted by w and l , respectively. Note that in the VKS2 device, these values are close to $w = 0.415$ (the presence of a copper inner wall may be modeled using $w = 0.45$) and $l = 0.385$, while w and l are taken as parameters in the numerical computations.

blades, which ensures a very efficient inertial stirring. The phenomenology of the mean flow is the following. Each impeller acts as a centrifugal pump: the fluid rotates with the impeller and is expelled radially by the centrifugal effect. To ensure mass conservation the fluid is pumped in the center of the impeller and recirculates near the cylinder wall. In the exact counter-rotating regime, the mean flow is divided into two toric cells separated by an azimuthal shear layer. The integral Reynolds number for this experiment is of the order of 10^7 and the shear layer instability is a strong source of turbulence.

In the first version of this experiment, called "VKS1", the achieved magnetic Reynolds number R_m was below the numerical prediction for criticality, computed for the time-averaged flow [14], and no self-excitation of a magnetic field was observed. Various measurements of induced magnetic field have been performed [10,11,12], showing a good agreement with preceding numerical predictions. In a second version (VKS2), which is still under commissioning, a higher motor power (300 kW) was installed. A careful optimization of the

time-averaged flow has been carried out, using a water-model experiment and varying the design of the driving impellers [13]. A solution achievable in the experimental device VKS2 has been found. This solution is based on the adjunction of a layer of stationary conductor surrounding the flow, which was supposed to reduce the critical magnetic Reynolds number R_m^c by a factor of 4. It will be called "side layer" and its thickness will be denoted by w in the following.

The kinematic dynamo simulations were carried out with a code that uses periodic boundary conditions in axial direction [13,14], what has to be considered as a compromise. Of course, the correct implementation of magnetic boundary conditions for non-spherical bodies has been a longstanding problem in dynamo research. Only recently, new methods and codes have been proposed to overcome this problem [15,16,17,18,19,20,21].

One of the goals of this paper is to apply two of those recently established numerical schemes to the design of cylindrical fluid dynamos, such as the VKS dynamo, and to compare their results with the results obtained with the periodic code. These two codes will be shortly described in section 2. The first one is a finite-difference scheme coupled to a solver of the Laplace equation in the external vacuum region, which had been successfully used in the simulation of the Riga dynamo experiment [9,15]. The second one is a code based on the integral equation approach for dynamos in finite domains [16,18,20] which basically relies on the self-consistent treatment of Biot-Savart's law.

These two codes will first be applied to an analytical test flow in section 3. Interestingly, we will see that the results obtained by the two codes do not differ significantly from those obtained with the periodic code.

Furthermore, these two non-periodic codes allow a more realistic treatment of the VKS dynamo system. We obtained surprising and unsettling results when taking into account the geometry of the vessel in the axial direction behind the impellers (section 4). This is characterized by the existence of layers of liquid sodium between the impellers and the end walls (the "lids") of the cylindrical vessel (Fig. 1). In the following, these layers will be referred as "lid layers", in distinction from the "side layers" at the envelope of the cylinder. We will see that even the mere existence of static lid layers increases the critical magnetic Reynolds number R_m^c by some 12 per cent. This is already a remarkable result as it shows, contrary to common wisdom [22,23], that *even for non-oscillatory* eigenfields the existence of conducting layers is not always advantageous for the dynamo to work (for *oscillatory* eigenfields, the possible deterioration of the dynamo condition with increasing layer thickness was discussed in [24,25]). The most dramatic effect occurs, however, when some rotational flow is assumed in the lid layer, which must be considered as naturally driven by the impeller. Then, even values of R_m^c close to 130 can be

found depending on the details of the assumed flow there.

The paper closes with a discussion of the results and with proposals how to overcome the indicated problems by constructional add-ons.

2 The utilized numerical codes

As stated in the first section, the periodic magnetic boundary conditions are easy to implement and the simplicity of the resulting kinematic dynamo code allows parametric studies without involving much numerical resources. This pseudo-spectral code with *periodic* boundary conditions for the magnetic field [26,13,14], which uses the Adams-Bashforth method for the time-stepping, will be denoted by "PER" in the following. As the real experiments take place obviously in a finite cylindrical container, it is particularly interesting to numerically verify if R_m^c for a flow configuration which is optimal in the periodic case is a robust quantity when the magnetic boundaries become finite. For this purpose, we have employed two different codes. The first one, henceforth referred as the *differential equation approach* (DEA), relies on the induction equation

$$\frac{\partial \mathbf{B}}{\partial t} = \nabla \times (\mathbf{u} \times \mathbf{B}) + \frac{1}{\mu_0 \sigma} \Delta \mathbf{B} , \quad (1)$$

wherein \mathbf{B} is the magnetic field and \mathbf{u} the velocity field. In this paper we will restrict our attention to axisymmetric flows which allows a decoupled treatment of the azimuthal modes $\sim \exp(im\varphi)$ of the magnetic field. Focusing on the azimuthal mode with $m = 1$, which is known to be the dominant mode for the VKS dynamo, the DEA code is a finite difference solver with a non-uniform grid in radial and axial direction. The time evolution is realized as an Adams-Bashforth scheme. The vacuum boundary conditions are implemented in such a way that for each time step the Laplace equation in the outer part is solved (by pseudo-relaxation), whereafter the resulting external solution is matched to the inner solution via the continuity demands for the tangential electric field components and the divergence free condition for the magnetic field. This code was already used successfully for the prediction and optimization of the Riga dynamo experiment [9,15].

The second code is based on the *integral equation approach* (IEA) to dynamos in finite domains, which had been developed and qualified for real problems during the last years [16,18,20]. Basically, it uses the three coupled integral equations

$$\begin{aligned}
\mathbf{B}(\mathbf{r}) = & \frac{\mu_0\sigma}{4\pi} \iiint_V \frac{(\mathbf{u}(\mathbf{r}') \times \mathbf{B}(\mathbf{r}')) \times (\mathbf{r} - \mathbf{r}')}{|\mathbf{r} - \mathbf{r}'|^3} dV' \\
& - \frac{\mu_0\sigma}{4\pi} \iint_S \phi(\mathbf{s}') \mathbf{n}(\mathbf{s}') \times \frac{\mathbf{r} - \mathbf{s}'}{|\mathbf{r} - \mathbf{s}'|^3} dS' \\
& - \frac{\mu_0\sigma\lambda}{4\pi} \iiint_V \frac{\mathbf{A}(\mathbf{r}') \times (\mathbf{r} - \mathbf{r}')}{|\mathbf{r} - \mathbf{r}'|^3} dV' , \tag{2}
\end{aligned}$$

$$\begin{aligned}
\frac{1}{2}\phi(\mathbf{s}) = & \frac{1}{4\pi} \iiint_V \frac{(\mathbf{u}(\mathbf{r}') \times \mathbf{B}(\mathbf{r}')) \cdot (\mathbf{s} - \mathbf{r}')}{|\mathbf{s} - \mathbf{r}'|^3} dV' \\
& - \frac{1}{4\pi} \iint_S \phi(\mathbf{s}') \mathbf{n}(\mathbf{s}') \cdot \frac{\mathbf{s} - \mathbf{s}'}{|\mathbf{s} - \mathbf{s}'|^3} dS' \\
& - \frac{\lambda}{4\pi} \iiint_V \frac{\mathbf{A}(\mathbf{r}') \cdot (\mathbf{s} - \mathbf{r}')}{|\mathbf{s} - \mathbf{r}'|^3} dV' , \tag{3}
\end{aligned}$$

$$\begin{aligned}
\mathbf{A}(\mathbf{r}) = & \frac{1}{4\pi} \iiint_V \frac{\mathbf{B}(\mathbf{r}') \times (\mathbf{r} - \mathbf{r}')}{|\mathbf{r} - \mathbf{r}'|^3} dV' \\
& + \frac{1}{4\pi} \iint_S \mathbf{n}(\mathbf{s}') \times \frac{\mathbf{B}(\mathbf{s}')}{|\mathbf{r} - \mathbf{s}'|} dS' . \tag{4}
\end{aligned}$$

The magnetic field \mathbf{B} is determined by the volume integral equation (2) which is a rewritten form of Biot-Savart's law. The vacuum boundary conditions are ensured by the surface integral equation (3) for the electric potential ϕ , which results from applying Green's theorem to the solution of the Poisson equation. Equations (2) and (3), with the third terms on the r.h.s. omitted, are sufficient for treating steady dynamo problems. In the unsteady case, for which we assume a time dependence $\sim \exp(\lambda t)$ for all electromagnetic quantities, they have to be completed by the additional equation (4) for the vector potential \mathbf{A} .

Accordingly, we have implemented two versions of the IEA approach. The first one [18], using only Eqs. (2) and (3), is an integral equation eigenvalue solver for R_m^c which works properly only if the critical eigenmode is non-oscillatory, otherwise it yields unphysical solutions with complex R_m^c . The second version [20] is an integral equation eigenvalue solver for the complex time constant λ , whose real part is the growth rate, and whose imaginary part is the angular frequency of the magnetic eigenmode.

As in the DEA case, the magnetic field \mathbf{B} , the electric potential ϕ and the vector potential \mathbf{A} are expanded in azimuthal modes $\sim \exp(im\varphi)$. The reduction of the equation system (2-4) to the dominant mode with $m = 1$ is complicated and will be published elsewhere. A few more remarks on this reduction can be found in the appendix.

3 An analytical test example

For the sake of comparison with existing results, and to get a first feeling on the role of lid layers, we have carried out some computations for an analytical test flow that was proposed and treated in [27,13]. The topology of this flow, denoted by s2t2 [28], is the same as in the real VKS experiment, consisting of two counter-rotating toroidal eddies (t2) and two poloidal rolls (s2). The flow is defined by the following velocity field in a cylindrical volume with $0 \leq r \leq 1$ and $-1 \leq z \leq 1$:

$$v_r = -\frac{\pi}{2}r(1-r)^2(1+2r)\cos(\pi z) , \quad (5)$$

$$v_\varphi = 4\epsilon r(1-r)\sin(\pi z/2) , \quad (6)$$

$$v_z = (1-r)(1+r-5r^2)\sin(\pi z) . \quad (7)$$

For the parameter ϵ which determines the ratio of toroidal to poloidal flow, we have used the same value $\epsilon = 0.7259$ as in [13]. It is important to note that at the envelope of the cylinder all three components v_r , v_φ and v_z vanish while at the top and the bottom v_r and v_φ do not vanish. Usually, the effect of any conducting layer around a dynamo depends strongly on the existence or non-existence of velocity components at the boundary.

Hereafter, we will always use the following definition of the magnetic Reynolds number:

$$R_m = \mu_0 \sigma r_1 v_{max} \quad (8)$$

where r_1 is the radius of the inner cylinder and v_{max} is the maximum velocity of the flow.

For the flow field according to Eqs. (5-7), Ravelet et al. found values of $R_m^c = 58$ for side layer thickness $w = 0$, and $R_m^c = 43$ for $w = 1$ [13]. These results were also confirmed by an independent Galerkin code [27].

In the DEA code, we have used a total of 119 grid points in z direction and 50 grid points in r direction. 65 of the grid points in z direction are in the internal part, the remaining 54 are outside. For $w = 0$, 21 of the grid points in r direction are in the internal part, the remaining 29 are outside. For $w = 1$, 39 of the grid points in r direction are in the internal part, the remaining 11 are outside. In the IEA code with $w = 0$, we have used a 20 x 20 grid in r and z direction. For $w = 1$, we have used 26 grid points in r direction and 18 grid points in z direction.

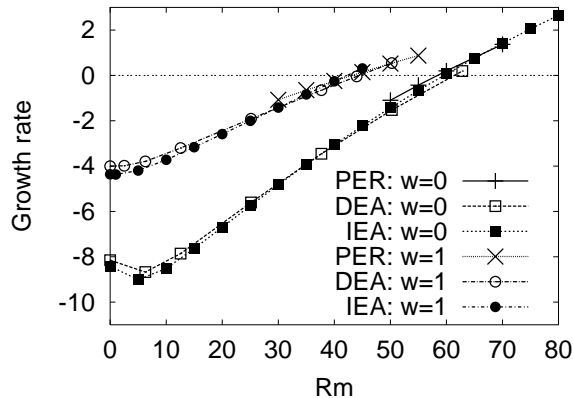


Fig. 2. Growth rates for the analytical test flow, with side layer thicknesses $w = 0$ and $w = 1$, as computed by the PER, DEA, and IEA code.

Table 1

R_m^c as computed for the analytical test flow with two side layer thicknesses w by three different codes explained in the text.

| Code | w | R_m^c |
|------|-----|---------|
| PER | 0.0 | 58 |
| DEA | 0.0 | 61.5 |
| IEA | 0.0 | 59.6 |
| PER | 1.0 | 43 |
| DEA | 1.0 | 44.5 |
| IEA | 1.0 | 42.3 |

In Fig. 2 we show the computed growth rates for the cases $w = 0$ and $w = 1$. The critical values for all three cases are summarized in Table 1. For $w = 0$, the DEA code gives $R_m^c = 61.5$, the IEA code gives $R_m^c = 59.6$. For $w = 1$, the DEA code gives $R_m^c = 44.5$, the IEA code gives $R_m^c = 42.3$. Interestingly enough, all three codes (PER, DEA, and IEA) give comparable results, which are $R_m^c = 59.8 \pm 1.8$ for $w = 0$ and $R_m^c = 43.4 \pm 1.1$ for $w = 1$.

The following conclusions can be drawn: For the considered analytical flow of the s2t2 type, the results of the DEA and the IEA code coincide quite remarkably, despite some differences in the used grid spacing. What is more, our results for R_m^c differ only slightly from the results that were obtained before by the PER code. This agreement may be related to the fact that the mirror-antisymmetry of the magnetic eigenfield within the enlarged elementary cell of the PER code ensures that no currents can leave the flow region [13], which is indeed a necessary boundary condition for the finite cylinder. Although this correspondence might be a bit special for the considered s2t2 flow, it is

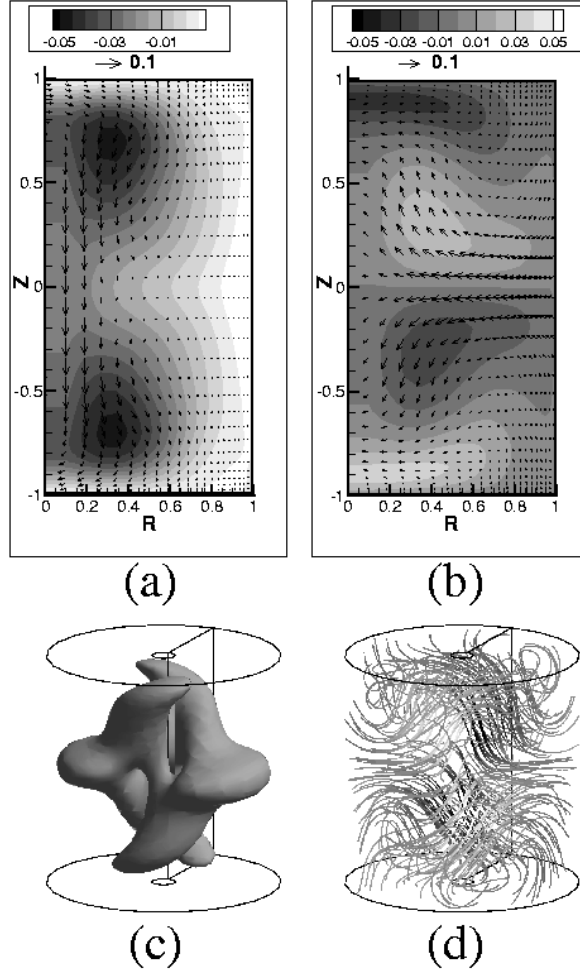


Fig. 3. (a,b) Poloidal field (arrows) and toroidal field (gray scale) in two azimuthal planes (rotated by 90 degrees), computed with the DEA code for the analytical test flow. (c) Isosurface of the magnetic field energy (25 per cent of maximum). (d) Magnetic field lines, computed with the IEA code. The gray scale indicates the axial component of the field. Note that the rotation axis is vertical, contrary to Fig. 1 and to the real VKS experiment where it is horizontal.

nevertheless remarkable. Its simplicity and reproducible dynamo behaviour might qualify the analytical flow (5-7) as a benchmark for other kinematic dynamo codes in cylindrical geometry.

For the case $w = 0$, the structure of the magnetic eigenfields is illustrated in Fig. 3. We show the poloidal and toroidal field structure in two azimuthal planes (Fig. 3a and 3b), which are rotated by 90 degree with respect to each other. Figures 3c and 3d give impressions of the 3D structure of the fields. In Fig. 3c we exhibit the isosurface (25 per cent of the maximum value) of the magnetic field energy, Fig. 3d gives an impression of the magnetic field lines. This eigenfield in form of an equatorial dipole was already discussed in [13] where also the structure of the electric currents is illustrated.

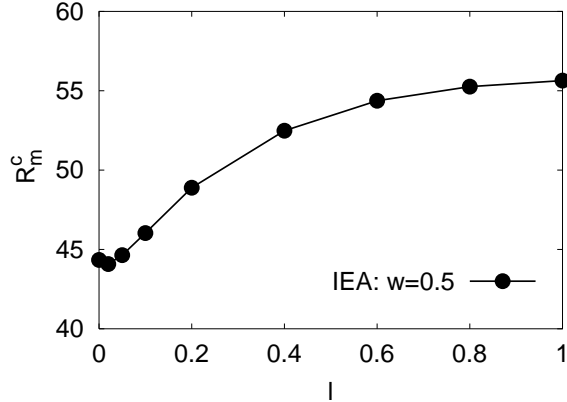


Fig. 4. Dependence of R_m^c on the thickness l of a stagnant lid layer for the analytical test flow with fixed side layer thickness $w = 0.5$.

Let us consider now the influence of a static lid layer on R_m^c , which is documented in Fig. 4 for the IEA code. We observe first a slight decrease of R_m^c only for very small lid layer thicknesses l , while for larger l the dynamo condition deteriorates. For $l = 1$ we get an increase of R_m^c by approximately 20 per cent, compared to the value at $l = 0$. Note that the PER code, which uses Fourier transforms in axial direction, is not very convenient for the handling of sharp velocity gradients. Nevertheless, a few numerical tests with this code have qualitatively confirmed the general tendencies observed with the DEA and IEA code.

This negative influence of lid layers on the dynamo is quite in contrast to the well-known positive effect of side layers [22,23]. Since such lid layers are indeed present for technical reasons in the VKS2 experiment, it is interesting to examine their role in more detail.

4 The VKS flow

After having considered an analytical test flow, we switch over now to the flow of the real VKS experiment. We have used the time-averaged flow field of the propeller "TM73" which was identified as the optimal flow field in [13], according to the periodic code. After making some interpolations to project this flow field onto the grids used in our DEA and IEA codes, we have investigated the influence of side layers and, in particular, the influence of lid layers and a possible flow therein on the dynamo condition.

In Table 2 we present a summary of the different lid layer and flow settings that were considered numerically, and indicate the resulting R_m^c . As before, DEA and IEA refer to the codes based on the differential equation approach and on the integral equation approach. w is the thickness of the side layers, l

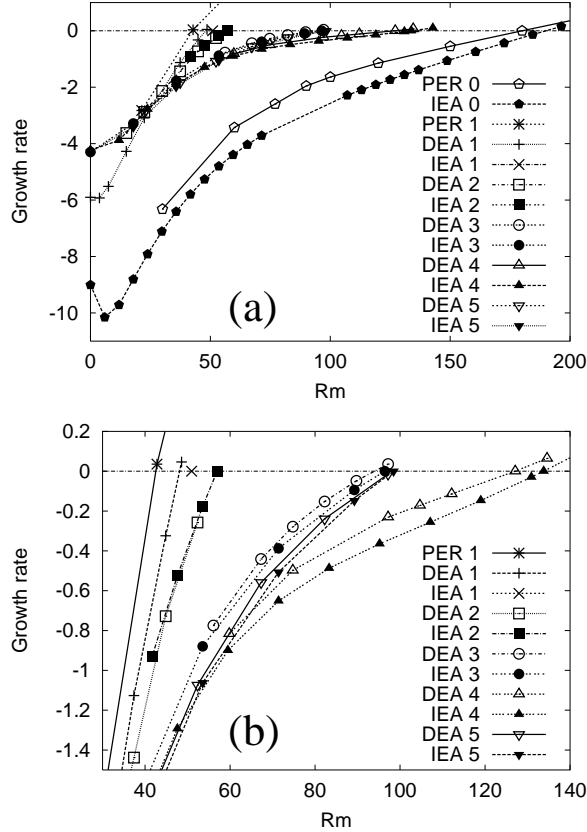


Fig. 5. Growth rates for the flow in the VKS experiment, as computed with the DEA and the IEA code for different settings of the lid layers and the flow structure therein. (b) is a zoom of (a). The results for PER 0 and PER 1 are also included. See Table 2 for further details.

the thickness of the lid layer. For numerical reasons, in some configurations a certain smoothing of the velocity field in transition regions has been employed. Probably, this will add to the differences between the results of DEA and IEA.

In Fig. 5, we have compiled the main results. Both parts of the figure show mainly the same growth rate curves, with more details visible in Fig. 5b.

The first observation concerns the very high value $R_m^c = 190$ for IEA 0, which represents the case that neither a lid layer nor a side layer is present. A similar value of 180 had been obtained with the periodic code [13], and the corresponding growth rate curve is indicated as PER 0 in Fig 5a. By adding a side layer the DEA 1 and IEA 1 values drop to approximately 50 which is not far from the PER 1 result 43. We see that now the effect of the side layer on R_m^c is much more significant than for the analytical test flow. The reason for this difference between both gains was already discussed in [13].

Assume now the side layer thickness to be fixed to $w = 0.45$, and consider the dependence of R_m^c on the lid layer thickness l , first without any flow therein.

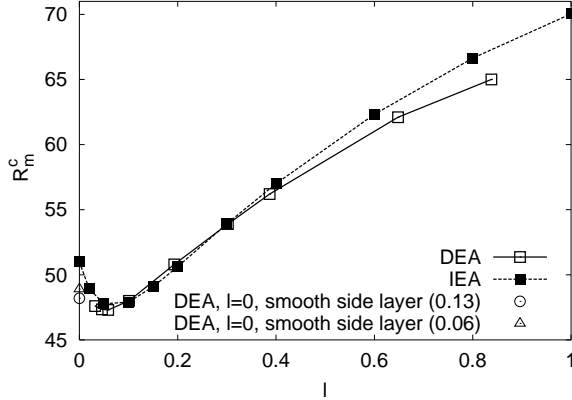


Fig. 6. Growth rates for the flow in the VKS experiment, as computed with the DEA and the IEA code for different thicknesses l of a stagnant lid layer. At $l = 0.4$ we obtain the cases DEA 2 and IEA 2 described in Table 2. The two individual points for DEA at $l = 0$ correspond to a smoothing of the velocity field between $r = 1$ and $r = 1.13$ or $r = 1.06$, respectively.

This dependence is given in Fig. 6.

Apart from a technical detail for the DEA code which requires, for $l = 0$, some smoothing of the velocity at $r = 1$, the IEA and DEA curves are in good correspondence, with slightly larger deviations for higher values of l . Again we observe a minimum of R_m^c close to $l = 0.05$, indicating that a thin lid layer of liquid sodium behind the propeller might be advantageous for the dynamo. However, with further increasing l this benefit is lost again, and for the (nearly) real value $l = 0.4$ we get $R_m^c = 56$ (DEA 2) and $R_m^c = 57$ (IEA 2) which is approximately 12 per cent above the value for $l = 0$. This seems to be not very much, but in terms of the necessary power consumption (which scales like $\sim R_m^3$) it would amount to an increase of 40 per cent.

This negative effect becomes much more dramatic when we consider the possibility of some flow in the lid layers. It is reasonable to assume at least some rotation in these layers due to the viscous coupling with the impeller. Up to now, this flow in the lid layers has not been measured, and it was not considered in the previous simulations with the periodic code, which is probably less suited to handle steep velocity gradients.

We study here two simplified flow patterns in the lid layers which are, at least, not completely unrealistic.

The first flow is basically a rotation which is linearly decaying from the impeller positions at $z = \pm 0.9$ until the walls at $z = \pm 1.3$. For numerical reasons we have assumed also a smoothing of v_r between $z = \pm 0.9$ and $z = \pm 1.0$ (in DEA 3 and IEA 3), and between $z = \pm 0.9$ and $z = \pm 0.95$ (in DEA 4). In IEA 4, a sharp decrease to zero of v_r at $z = \pm 0.9$ has been assumed. The effects are

astonishing. For DEA 3 and IEA 3 we get a R_m^c of 94 and 97, respectively. For DEA 4 we get 128, and for IEA 4 we get 133. Apart from the fact that the rotational flow drives R_m^c to forbidding high values there is also a strong sensitivity on the precise form of v_r at the impeller position.

The second flow pattern is a rotation which is assumed constant between the impeller and the wall. The resulting R_m^c is 98, both for DEA 5 and IEA 5. Note that in this case also a smoothing of v_r between $z = \pm 0.9$ and $z = \pm 1.0$ was used.

As this "lid effect" was not noticed before and may prove dangerous for any experimental fluid dynamos driven by counter-rotating impellers, we will try in the following to give more details on the balance between magnetic generation and dissipation. For this it is useful to analyze, by taking values from IEA 2, IEA 3, and IEA 4, a few global characteristics which are essential for the efficiency of dynamos. From the r.h.s of Eq. (1) we read off that the dynamo effect is governed by the competition of magnetic field production (the first term) and dissipation (the second term). Therefore we will consider in the following the normalized dissipation rate D and the normalized production rate P , defined by

$$D = \frac{\int |\nabla \times \mathbf{B}|^2 dV}{\int |\mathbf{B}|^2 dV}, \quad (9)$$

$$P = \frac{\int [(\nabla \times \mathbf{B}) \times \mathbf{B}] \cdot \mathbf{u} dV}{\int |\mathbf{B}|^2 dV}, \quad (10)$$

respectively.

The dependence of these quantities, and of their ratio, on the lid layer thickness l is shown in Fig. 7, together with the corresponding R_m^c .

For each of the settings, IEA 2, IEA 3, and IEA 4, we observe initially (between $l = 0$ and $l = 0.1$), a decrease of the dissipation D , which is not completely compensated by a decreasing field production P . As a result, we get a decrease of D/P and hence of R_m^c . For larger l , however, D increases again. In particular for IEA 3 and IEA 4 it is interesting to see that P remains rather constant. For IEA 4, D becomes very large for $l = 0.4$ which leads to the high value of $R_m^c = 133$. Note that these global results for production and dissipation strongly differ from the ones obtained with a side layer of variable thickness (see figure 19 in [13]).

In the following, we will analyze the impact of lid layers on the radial, azimuthal and axial components of the dissipation term. We see in Fig. 8 that the radial and the axial currents contribute relatively little to the total dissipation, and that this contribution does not change significantly with increasing l .

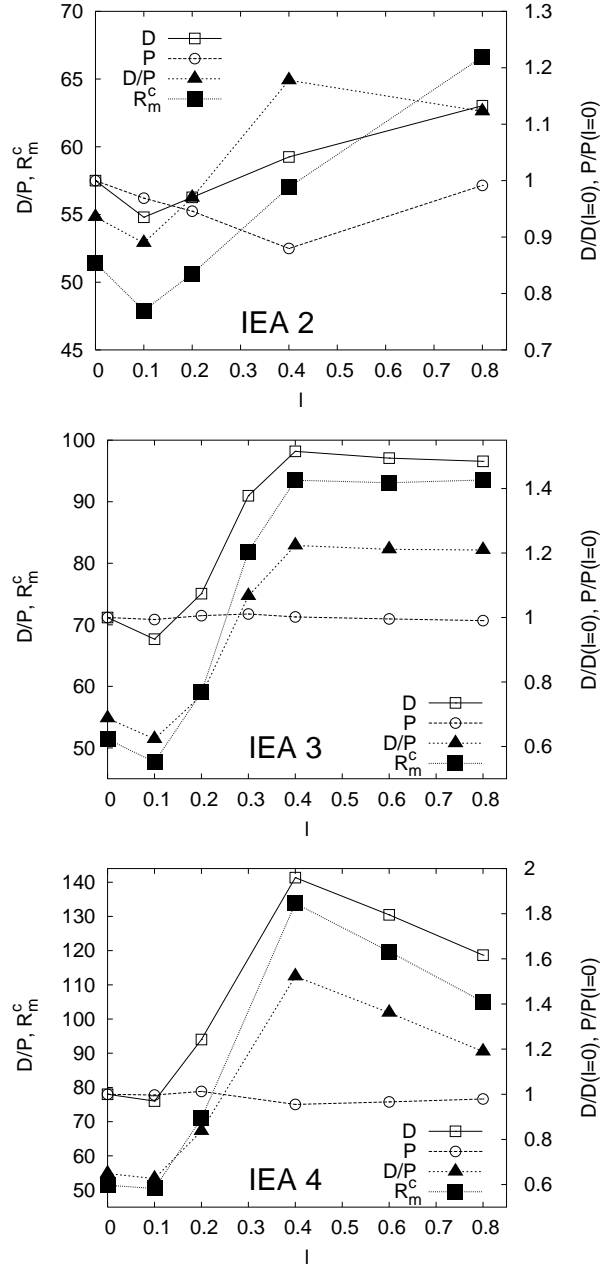


Fig. 7. Dissipation rate D , production rate P (both normalized to the value at $l = 0$), ratio D/P , and R_m^c in dependence on the thickness l of the lid layer. From the top: IEA 2, IEA 3, IEA 4. Note the fact that the ratio D/P and R_m^c are approximately the same.

The dominant dissipation, which comes from the azimuthal current, strongly increases for IEA 3 and IEA 4 with increasing l .

Having identified the azimuthal current as the "main offender" for the observed high R_m^c , let us consider it more in detail. For this purpose, we show in Fig. 9 the radially averaged value of j_φ^2 , again normalized with the total magnetic

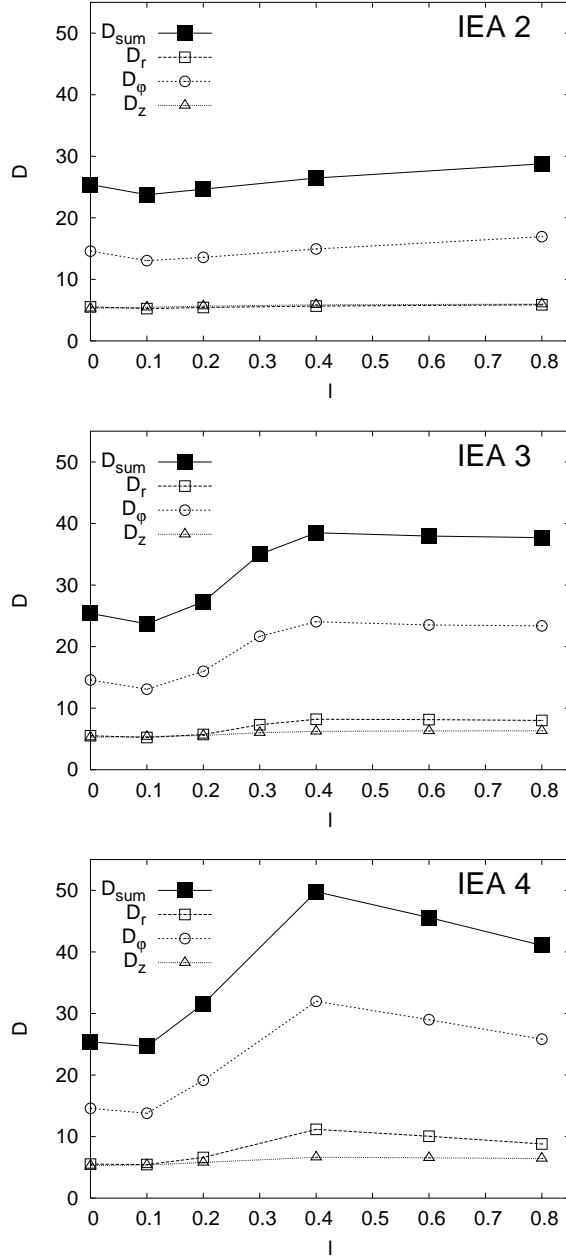


Fig. 8. Individual dissipation rates resulting from the radial, the azimuthal and the axial current, and their sum. From the top: IEA 2, IEA 3, IEA 4.

energy, in dependence on z (note that this picture is symmetric for negative z). As expected, nothing special happens for IEA 2, but for IEA 3 and even more for IEA 4 we see a strong enhancement, in particular between $z = 0$ and $z = 0.2$.

We know that j_ϕ depends both on the radial derivative of B_z and the axial derivative of B_r . For that reason, the radial average of B_r^2 in dependence on z and the axial average of B_z^2 in dependence on r are depicted in Fig. 10. We

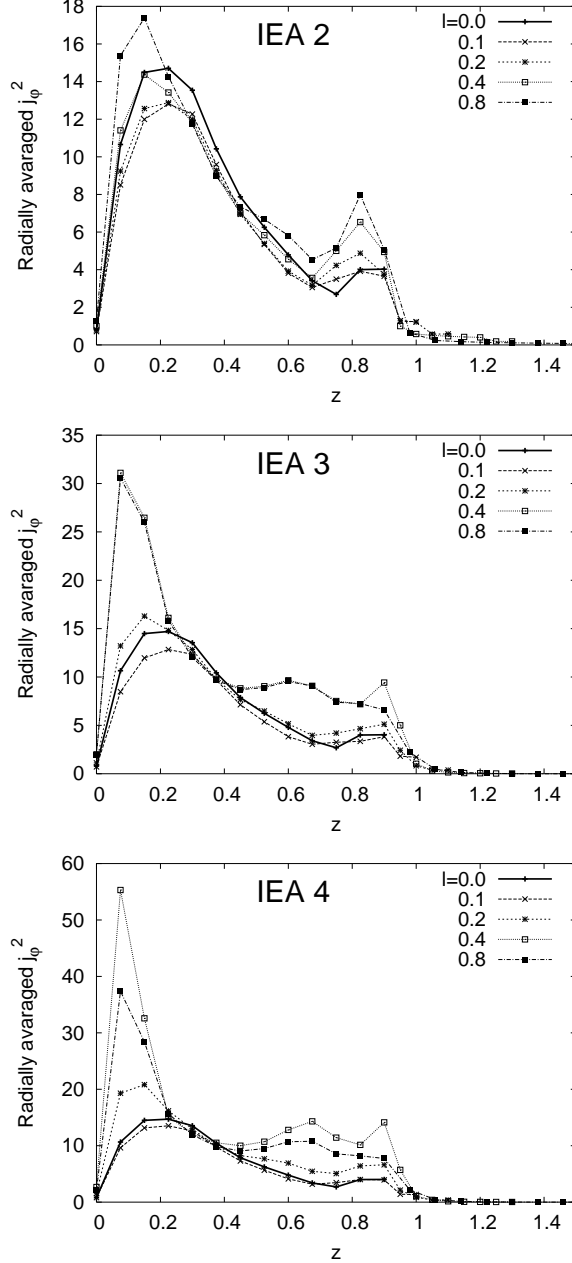


Fig. 9. $\int_0^{R+w} j_\varphi^2 r dr / (\int |\mathbf{B}|^2 dV)$ in dependence on z . From the top: IEA 2, IEA 3, IEA 4. Note the different scales of the axis of ordinates.

see that both fields contribute to the enhancement of j_φ .

This is also visible in the magnetic field plots of Fig. 11, which shows again two azimuthal planes. Differing from the previous plots, we have chosen here the settings IEA 1, IEA 2, and IEA 4. In the latter (Fig. 11f) we see nicely how B_z acquires strong radial gradients. It seems that B_z is compressed into a small radial stripe, an effect that contributes strongly to the high azimuthal current and hence to high dissipation there.

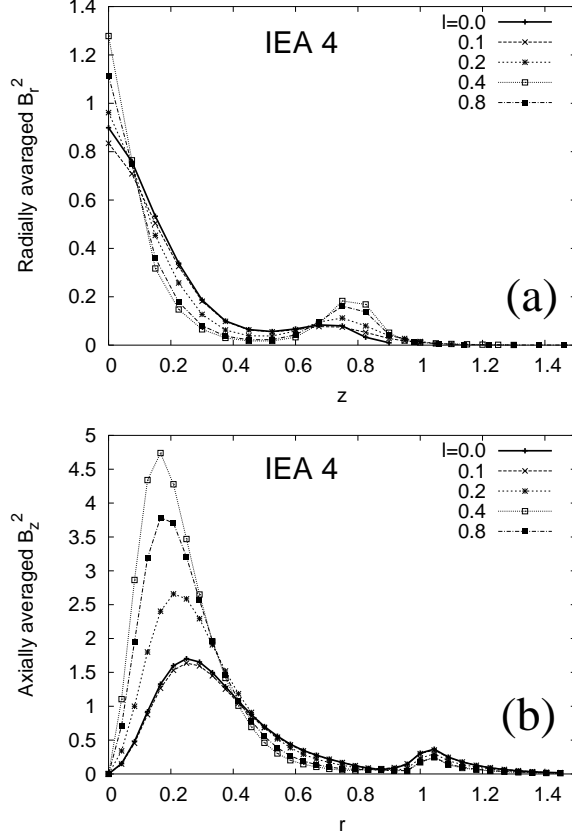


Fig. 10. Explanation of the strongly enhanced azimuthal currents by the magnetic field components for IEA 4. (a) $\int_0^{R+w} B_r^2 r dr / (\int |\mathbf{B}|^2 dV)$ in dependence on z for different lid layer thicknesses l . Note the stronger gradients for $l = 0.4$ and $l = 0.8$. (b) $\int_{-H-l}^{H+l} B_z^2 dz / (\int |\mathbf{B}|^2 dV)$ in dependence on r .

5 Discussion

In this paper, we have found a strong influence of lid layers and, even more pronounced, of the flow structure therein on the self-excitation threshold for von Kármán type dynamos. For the realistic VKS geometry, and taking into account only static lid layers, we obtained an increase of R_m^c by around 12 per cent. Allowing the azimuthal velocity to decay linearly to zero between the impeller and the top and the bottom walls, or allowing it to be constant between the impeller and the walls, leads to an increase of R_m^c by 100 per cent to values around 95 or even by 150 percent to 133, depending on other flow details. Apart from accuracy questions in the order of a few per cent, these results should be considered as rather reliable, since both the DEA and the IEA code yield basically the same values and eigenfunctions.

It would be tempting to illustrate this behaviour in simple terms. Consider a cylinder of height H and radius r . Assume, for the moment, uniform currents

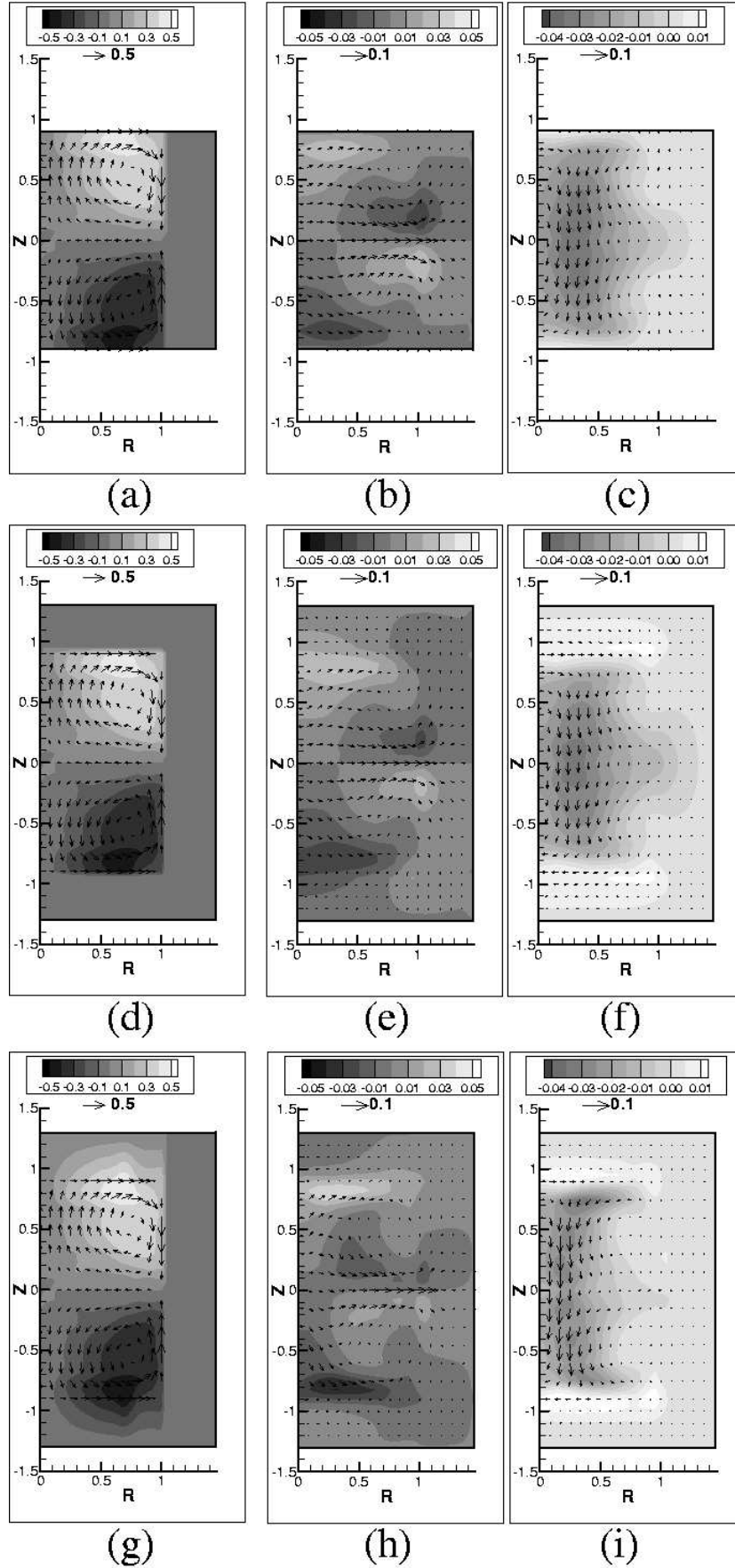


Fig. 11. Velocity field (left column) and magnetic field structure in two azimuthal planes (middle and right column) for the VKS experiment, assuming different lid layer configurations. (a,b,c) IEA 1. (d,e,f) IEA 2. (g,h,i) IEA 4.

flowing in axial, radial and azimuthal directions. For those, we may define individual radial (R_r), azimuthal (R_φ), and axial (R_z) resistances:

$$R_r = 1/(2\pi\sigma H) , \quad (11)$$

$$R_\varphi = \pi/(\sigma H) , \quad (12)$$

$$R_z = H/(\sigma\pi r^2) . \quad (13)$$

When a stagnant *lid* layer ($l \neq 0$) is added at both ends of the cylinder, the height H of the cylinder becomes larger. From Eqs. (10-12), one can see that R_r and R_φ decrease and R_z increases with H . For small layer thicknesses the azimuthal and radial currents would still be dominant, hence the whole dissipation should decrease. But if the axial current becomes stronger, the dissipation would increase. Under the assumption that the production rate did not change too much, R_m^c should show a similar behaviour. In contrast to that, if we add a stagnant *side* layer ($w \neq 0$), the radius r increases and the height H of the cylinder remains unchanged. For this situation, from Eqs. (11-13) one reads off that R_r and R_φ would not change, but R_z would decrease. If we assumed the production rate to have no significant change, R_m^c should always decrease. Therefore, one could hope that the different scalings of Eqs. (11-13) with H and r might already reflect the main difference that lid layers and side layers have on the dynamo condition.

Unfortunately, the reality seems not to be such simple. If those scaling arguments were correct, Fig. 8a should show a decreasing (with l) D_φ (and D_r), and an increasing D_z . In reality, however, both the minimum and the following increase rely exclusively on the behaviour of D_φ while D_z (and D_r) do not play any significant role.

By following, in section 4, the trace from enhanced dissipation via increased azimuthal current, we have identified the strong steepening of the axial and radial field components in the central bulk of the dynamo as the main reason for the dramatic increase of R_m^c . Hence, the deterioration of the dynamo condition does not rely, as could be hypothesized, on an increased dissipation *in the added lid layer*, but on the change of the eigenmode structure *in the bulk* of the dynamo.

What could be a technical consequence for the real VKS experiment if R_m^c increases significantly due to the lid effect? Provided that the kinematic dynamo results based on the time-averaged flow still apply, in essence, to the turbulent VKS2 flow, the installed motor power will not allow anymore the observation of dynamo action, since the driving power scales as the cube of the magnetic Reynolds number. One could thus try, first, to avoid any flow behind the impeller by some simple inserts or blades. But this would lead, at the best, to an $R_m^c \sim 57$ for the actual value $l = 0.4$. The best solution of the lid layer problem might be to install additional steel housings between the

Table 2

Table with different side/lid layer and flow configurations for the VKS flow with propeller TM 73, and the computed R_m^c . Note that the experimentally achievable R_m is approximately 55. The "side layer smoothing", which means a linear decay to zero of the velocity between $r = 1$ and $r = 1.1$, has no significant effect on R_m^c . In contrast to this, smoothing of v_r in the lid layer has drastic effects (cp. the difference of DEA/IEA 3 and DEA/IEA 4.)

| Model | w | Side layer smoothing | l | v_φ in lid layer | Smoothing of v_r in lid layer | R_m^c |
|-------|------|----------------------|-----|-----------------------------------|------------------------------------|---------|
| PER 0 | 0 | - | 0 | - | - | 180 |
| IEA 0 | 0 | - | 0 | - | - | 190 |
| PER 1 | 0.4 | no | 0 | - | - | 43 |
| DEA 1 | 0.45 | yes | 0 | - | - | 48 |
| IEA 1 | 0.45 | no | 0 | - | - | 51 |
| DEA 2 | 0.45 | no | 0.4 | no | no | 56 |
| IEA 2 | 0.45 | no | 0.4 | no | no | 57 |
| DEA 3 | 0.45 | yes | 0.4 | Linear decay in $0.9 < z < 1.3$ | Linear decay in $0.9 < z < 1.0$ | 94 |
| IEA 3 | 0.45 | no | 0.4 | Linear decay in $0.9 < z < 1.3$ | Linear decay in $0.9 < z < 1.0$ | 96 |
| DEA 4 | 0.45 | yes | 0.4 | Linear decay in $0.9 < z < 1.3$ | Linear decay in $0.9 < z < 0.95$ | 128 |
| IEA 4 | 0.45 | no | 0.4 | Linear decay in $0.9 < z < 1.3$ | no | 133 |
| DEA 5 | 0.45 | yes | 0.4 | Constant in $0.9 < z < 1.3$ | Linear decay in $0.9 < z < 1.0$ | 98 |
| IEA 5 | 0.45 | no | 0.4 | Constant in $0.9 < z < 1.3$ | Linear decay in $0.9 < z < 1.0$ | 98 |

impellers and the end walls in order to hinder any sodium to go there ¹.

Another part of the problem which has not been considered yet is the presence of metallic driving impellers of finite conductivity. The conductivity jump between the fluid and the solid has not been implemented in the present DEA

¹ In this context it might be interesting to remind that the first dynamo of Lowes and Wilkinson became only operative after inserting a small amount of insulation to suppress a degenerative part of the induced currents [3].

and IEA codes (although there are no principle obstacles to do that). With the available codes, a thin layer of liquid sodium in solid rotation could also be an approximation of the real impeller. Since the tested rotating lid configurations led to threshold increase, one would generally expect an extra threshold increase for the complete problem. Thus, it seems favorable to use propellers of the smallest possible conductivity. But even a stainless steel impeller, which is less conducting than sodium, might still deteriorate the dynamo condition. A detailed investigation of this problems is left for future work.

Various experiments using MHD flows without internal walls are now in progress in the world, and one expects manifestation of dynamo action and nonlinear saturation under conditions closer to the natural astrophysical dynamos. In the case of the cylindrical VKS experiment, we have shown that an added layer (static or rotating) brings about surprizing consequences when situated in the lids area. These results suggest that the role of added layers be systematically studied for other flow configurations, both in order to empirically lower the critical magnetic Reynolds number and also to shed some light on the process of dynamo action.

Acknowledgments

This work was supported by Deutsche Forschungsgemeinschaft in frame of SFB 609 and Grant No. GE 682/12-2. We thank the French GdR Dynamo No 2060.

Appendix

In this appendix, we give a few indications how the three dimensional integral equation system (2-4) can be reduced to a two-dimensional one. We consider a cylinder with the radius R and height H . Introducing the cylindrical coordinate system (r, φ, z) , we have

$$\begin{aligned} \mathbf{r} &= [r \cos \varphi, r \sin \varphi, z]^T, \mathbf{r}' = [r' \cos \varphi', r' \sin \varphi', z']^T, \\ \mathbf{B} &= [B_r, B_\varphi, B_z]^T, \mathbf{u} = [u_r, u_\varphi, u_z]^T. \end{aligned} \tag{14}$$

The magnetic field \mathbf{B} , the electric potential ϕ , and the vector potential \mathbf{A} are expanded in azimuthal modes:

$$\begin{pmatrix} \mathbf{B} \\ \phi \\ \mathbf{A} \end{pmatrix} = \sum_{m=-\infty}^{\infty} \begin{pmatrix} \mathbf{B}_m \\ \phi_m \\ \mathbf{A}_m \end{pmatrix} \exp(im\varphi). \quad (15)$$

If the velocity field is axisymmetric, the equation system (2-4) is decoupled with respect to m . By introducing the six integrals

$$E_1^m(r, r', z, z') = \int_0^{2\pi} \frac{\cos m\varphi'}{(r^2 + r'^2 - 2rr' \cos \varphi' + (z - z')^2)^{\frac{3}{2}}} d\varphi', \quad (16)$$

$$E_c^m(r, r', z, z') = \int_0^{2\pi} \frac{\cos m\varphi' \cos \varphi'}{(r^2 + r'^2 - 2rr' \cos \varphi' + (z - z')^2)^{\frac{3}{2}}} d\varphi', \quad (17)$$

$$E_s^m(r, r', z, z') = \int_0^{2\pi} \frac{\sin m\varphi' \sin \varphi'}{(r^2 + r'^2 - 2rr' \cos \varphi' + (z - z')^2)^{\frac{3}{2}}} d\varphi', \quad (18)$$

$$D_s^m(r, r', z, z') = \int_0^{2\pi} \frac{\sin \varphi' \sin m\varphi'}{(r^2 - 2rr' \cos \varphi' + r'^2 + (z - z')^2)^{\frac{1}{2}}} d\varphi', \quad (19)$$

$$D_c^m(r, r', z, z') = \int_0^{2\pi} \frac{\cos \varphi' \cos m\varphi'}{(r^2 - 2rr' \cos \varphi' + r'^2 + (z - z')^2)^{\frac{1}{2}}} d\varphi', \quad (20)$$

$$D_1^m(r, r', z, z') = \int_0^{2\pi} \frac{\cos m\varphi'}{(r^2 - 2rr' \cos \varphi' + r'^2 + (z - z')^2)^{\frac{1}{2}}} d\varphi'. \quad (21)$$

over the angle φ' , all the three-dimensional integrals in Eqs. (2-4) can be reduced to two-dimensional integrals over r and z , and the two-dimensional integral can be reduced to a line integral.

Therefore, under the assumption that the velocity field is axisymmetric, the integral equation system (2-4) can be reduced to the two-dimensional case.

References

- [1] G. Rüdiger and R. Hollerbach, *The Magnetic Universe*, Wiley-VCH, Weinheim, 2004.
- [2] F.J. Lowes, I. Wilkinson, Geomagnetic dynamo: a laboratory model, *Nature* 198 (1963) 1158–1160.
- [3] I. Wilkinson, The contribution of laboratory dynamo experiments to our understanding of the mechanism of generation of planetary magnetic fields, *Geophys. Surveys* 7(1984) 107–122.

- [4] A. Gailitis, O. Lielausis, E. Platacis, G. Gerbeth, F. Stefani, Colloquium: Laboratory experiments on hydromagnetic dynamos, *Rev. Mod. Physics.* 74 (2002) 973–990.
- [5] A. Gailitis et al., Detection of a flow induced magnetic field eigenmode in the Riga dynamo facility, *Phys. Rev. Lett.* 84 (2000) 4365–4368.
- [6] A. Gailitis et al., Magnetic field saturation in the Riga dynamo experiment, *Phys. Rev. Lett.* 86 (2001) 3024–3027.
- [7] U. Müller, R. Stieglitz, Can the Earth’s magnetic field be simulated in the laboratory? *Naturwissenschaften* 87 (2000) 381–390.
- [8] R. Stieglitz, U. Müller, Experimental demonstration of a homogeneous two-scale dynamo, *Phys. Fluids* 13 (2001) 561–564.
- [9] A. Gailitis, O. Lielausis, E. Platacis, G. Gerbeth, F. Stefani, Riga dynamo experiment and its theoretical background, *Phys. Plasmas* 11 (2004) 2838–2843.
- [10] M. Bourgoin et al., Magnetohydrodynamics measurements in the von Kármán sodium experiment, *Phys. Fluids* 14 (2002) 3046–3058.
- [11] L. Marié et al., Open questions about homogeneous fluid dynamos: the VKS experiment, *Magnetohydrodynamics* 38 (2002) 163–176.
- [12] F. Pétrélis et al., Nonlinear magnetic induction by helical motion in a liquid sodium turbulent flow, *Phys. Rev. Lett.* 90 (2003) 174501.
- [13] F. Ravelet, A. Chiffaudel, F. Daviaud, J. Léorat, Towards an experimental von Kármán dynamo: numerical studies for an optimized design, *Phys. Fluids* 17 (2005) 117104.
- [14] L. Marié, J. Burguete, F. Daviaud, J. Léorat, Numerical study of homogeneous dynamo based on experimental von Kármán type flows, *Eur. Phys. J. B* 33 (2003) 469–485.
- [15] F. Stefani, G. Gerbeth, A. Gailitis, Velocity profile optimization for the Riga dynamo experiment, in: Alemany, A., Marty, Ph., Thibault, J.-P. (Eds.), *Transfer Phenomena in Magnetohydrodynamics and Electroconducting Flows*, Kluwer, Dordrecht, 1999, pp. 31–44.
- [16] F. Stefani, G. Gerbeth, K.-H. Rädler, Steady dynamos in finite domains: an integral equation approach, *Astron. Nachr.* 321 (2000) 65–73.
- [17] J.-L. Guermond, J. Léorat, C. Nore, A new Finite Element Method for magnetodynamical problems: two-dimensional results, *Eur. J. Mech. B* 22 (2003) 555–579.
- [18] M. Xu, F. Stefani, G. Gerbeth, The integral equation method for a steady kinematic dynamo problem, *J. Comp. Phys.* 196 (2004) 102–125.
- [19] A.B. Iskakov, S. Descombes, E. Dormy, An integro-differential formulation for magnetic induction in bounded domains: boundary element-finite volume method, *J. Comp. Phys.* 197 (2004) 540–554.

- [20] M. Xu, F. Stefani, G. Gerbeth, Integral equation approach to time-dependent kinematic dynamos in finite domains, *Phys. Rev. E* 70 (2004) 056305.
- [21] M. Bourgoin, P. Odier, J.-F. Pinton, Y. Ricard, An iterative study of time independent induction effects in magnetohydrodynamics, *Phys. Fluids* 16 (2004) 2529–2547.
- [22] E.C. Bullard, D. Gubbins, Generation of magnetic fields by fluid motions of global scale, *Geophys. Astrophys. Fluid Dyn.* 8 (1977) 43-56.
- [23] R. Avalos-Zuñiga, F. Plunian, Influence of inner and outer walls electromagnetic properties on the onset of a stationary dynamo, *Eur. Phys. J. B* 47 (2005) 127–135.
- [24] R. Kaiser, A. Tilgner, Kinematic dynamos surrounded by a stationary conductor, *Phys. Rev. E* 60 (1999) 2949–2952.
- [25] R. Avalos-Zuñiga, F. Plunian, A. Gailitis, Influence of electromagnetic boundary conditions onto the onset of dynamo action in laboratory experiments, *Phys. Rev. E* 68 (2003) 066307.
- [26] J. Léorat, Numerical simulations of cylindrical dynamos, *AIAA Progr. Astron. Aeron.* 162 (1994) 282–292.
- [27] L. Marié, C. Normand, and F. Daviaud, Galerkin analysis of kinematic dynamos in the von Kármán geometry, *Phys. Fluids* 18 (2004) 017102.
- [28] M.L. Dudley, R.W. James, Time-dependent kinematic dynamos with stationary flows, *Proc. R. Soc. Lond. A* 425 (1989) 407–429.